Update of key reactions in the low-temperature oxidation chemistry of dimethyl ether and analytic ignition delay times

M. Döntgen*, [1,2], J. Beeckmann[3], K. Leonhard[1,2], H. Pitsch[3], S.J. Klippenstein[4]

[1]Chair of Technical Thermodynamics, RWTH Aachen University, Germany
[2]AICES Graduate School, RWTH Aachen University, Germany
[3]Institute for Combustion Technology, RWTH Aachen University, Germany
[4]Chemical Sciences and Engineering Division, Argonne National Laboratory, United States

Abstract
Key reactions of the dimethyl ether low-temperature oxidation chemistry were updated based on an RRKM/ME study using high-level quantum mechanics. The updated kinetics were used to compute analytic ignition delay times and ignition delay times based on a reduced 36-step mechanism. The comparison to predictions of previous models and to experimental data at 13 bar shows the need for more holistic updates of reaction models.

Introduction

Dimethyl ether (DME) as a potential diesel fuel [1] has attracted great interest in combustion and atmospheric science due to its pronounced low-temperature oxidation chemistry. Although a large variety of experiments at both engine relevant [2-7] and ambient pressure conditions [8-12] and theoretical studies [13-18] have been dedicated to DME, the low-temperature pathways still require updates of their kinetic parameters. The present study addresses this need by calculating temperature dependent rate constants at 13 bar for key reactions of the low-temperature chemistry of DME. We make use of the recently established analytic solution of a global 4-step mechanism for computing the ignition delay time [19].

Directly after DME was proposed as a diesel fuel, high-pressure experiments by Pfahl *et al.* [2] and Dagaut *et al.* [3], as well as low-pressure experiments by Sehested *et al.* [8] revealed key aspects of the DME low-temperature chemistry. The negative temperature coefficient (NTC) regime observed for DME was assumed to be caused by RO_2 chemistry similar to that of long-chain hydrocarbons. Based on the first experimental data and parameter predictions, Curran *et al.* [20] reported the first detailed model for DME low-temperature oxidation. Subsequent updates by Fischer and Curran [21, 22] led to a widely used and accepted DME model for a wide temperature region, referred to as CF2000 in the following. Burke *et al.* [23] recently updated the Fischer/Curran model with recent experimental and theoretical data. Tomlin et al. [24] recently evaluated three different DME models based on global sensitivity analysis and pointed out the need for further investigation of the O_2 addition reactions of the DME low-temperature chemistry. Based on the CF2000 model, Beeckmann *et al.* [19] recently established a 36-step model and a global 4-step model for DME. The latter was solved analytically in order to deduce an analytical expression for ignition delay times.

The first detailed theoretical work on DME low-temperature oxidation was performed by Yamada et al. [13] using the CBS-q and G2 methods. Comprehensive theoretical kinetic studies have been performed by Andersen and Carter [14-17] using DFT for Born-Oppenheimer molecular dynamics simulations and for computing thermochemistry data, which has in turn been used in an RRKM/ME study. Recently, a combined experimental and theoretical work reported rate formulations for the first steps of the chain propagation mechanism of the low-temperature network of DME [18].

Theory has progressed substantially since the work of Andersen and Carter [14, 15] and the recent work of Eskola *et al.* [18] considered only a limited part of the kinetics. Thus, we aim to provide rate constants at a high level of theory using a master equation formulation of the low-temperature network of DME oxidation. By means of this formulation, Arrhenius expressions for the engine relevant temperature and pressure regime will be provided. Furthermore, the updated kinetics of key reactions will be used to determine analytical ignition delay times.

Methods

The RO2 to QOOH isomerization, the competing fates of QOOH, and the hydroxyl loss reactions were pointed out as key reactions [19]. We updated these key reactions for the low-temperature DME oxidation based on a RRKM/ME study using the PAPER software package [25]. Electronic structure and 2nd derivative calculations were performed with the B2PLYPD3 double hybrid functional and the 6-311++G(d,p) basis set using the Gaussian Software package [26]. Single point energy calculations were performed with the CCSD(T)-F12 method using the MOLPRO quantum chemistry package [27] and extrapolations of the VDZ-F12, VTZ-F12 and VQZ-F12 basis sets to the CBS limit were performed using a linear and a power extrapolation scheme [28, 29]. Coupled anharmonic effects of multiple internal hindered rotors were included at the

*Corresponding author: malte.doentgen@ltt.rwth-aachen.de

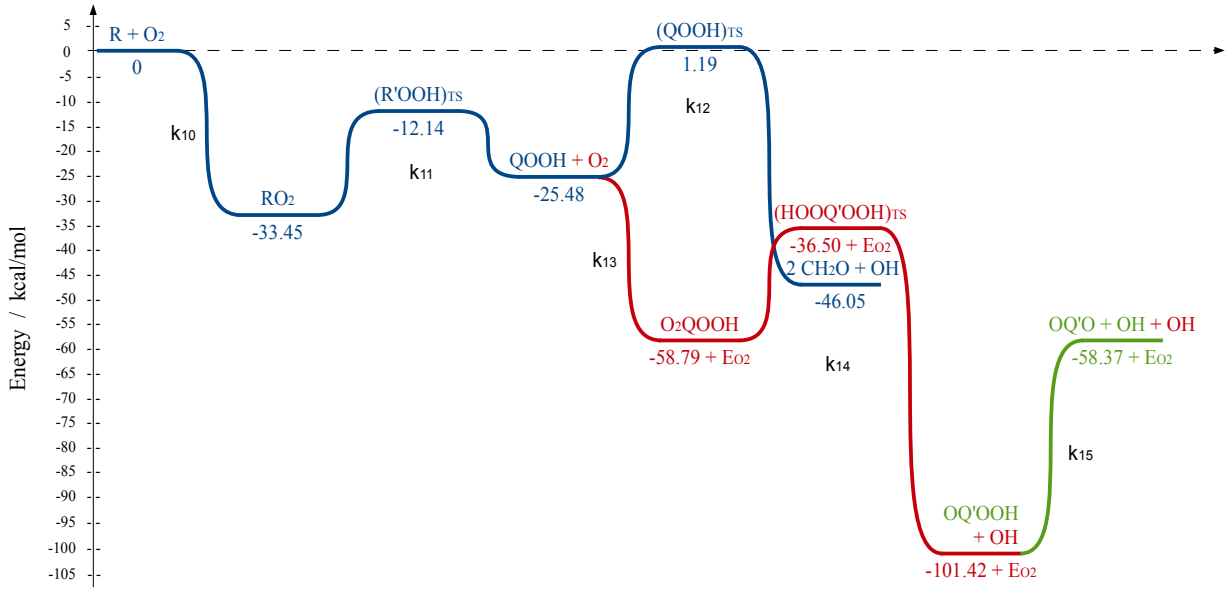

Figure 1: Master equation formulation of the RO_2 chemistry of DME. The colors indicate the different master equations used to investigate the key reactions of DME low-temperature chemistry. The full potential energy surface includes multiple competing pathways for QOOH and OQ'OOH, which are included in the formulation, but which are not significant for the present work. The k_{ij}'s give the IDs used in the discussion of rate constants.

B2PLYPD3/6-311++G(d,p) level to replace low harmonic frequencies of the respective rocking modes. The anharmonicity of umbrella motions in the CH_2 groups of R and QOOH have been neglected since their corresponding harmonic frequencies indicated that the harmonic approximation was accurate enough.

The thermochemistry of species and transition states was used to compute microcanonical rate constants using RRKM theory, including Eckart tunneling. The transition state partition function of the barrierless reactions was investigated using VRC-TST [30, 31]. The minimum energy path was determined at the CASPT2/cc-pVTZ level of theory (with a level shift of 0.2) for R + O_2 and with the smaller cc-pVDZ basis set for QOOH + O_2 and OQ'O + OH, using (7,5), (7,5) and (4,3) active spaces, respectively. In the latter active space, the mixing of the two near degenerate states of OH was included by using the multistate formulation of CASPT2 [32]. The molecular geometries used to compute single point energies of the interacting fragments at different distances were taken from the infinite separation case, *i.e.*, the non-interacting case. Corrections for the effect of close-range interactions on the molecular geometry were included. Furthermore, CCSD(T) single point energy corrections along the minimum energy path were included by shifting the doublet CASPT2 energy with the difference between the quartet CASPT2 and the quartet CCSD(T) single point energy. In addition, the single point energies were extrapolated to the CBS limit. Collisional kinetics were estimated based on collision parameters of propyl and argon. Thus, we used argon as a bath gas in the present study.

Analytic ignition delay times were computed based on the solution of a global 4-step mechanism of DME low-temperature oxidation [19]. This global 4-step mechanism was derived from a 36-step mechanism, which in turn was a reduction of the detailed CF2000 DME model [21, 22]. The formulation of the ignition delay time is given according to

$$t_{\mathrm{ign}} = \frac{1}{\lambda_1 k_{15,0}} \ln\left(\frac{0.05\, X_{\mathrm{F},0}\, \lambda_1 (\lambda_1 - \lambda_2)}{\varepsilon(\sigma/(1-\beta)+\lambda_1)(1-\lambda_2/\sigma)}\right) \quad (1)$$

where $X_{\mathrm{F},0}$ is the initial DME concentration, $k_{15,0}$ the second OH loss rate constant, $\lambda_{1/2}$ the eigenvalues of the solution, and ε, σ, β are concentration balance factors which can be taken from Ref. [19]. The validity of the analytic solution is checked by solving the 36-step mechanism including all six reactions discussed in the present work (*cf.* Figure 1), using the FlameMaster software package [33]. The reduction of the detailed CF2000 model to the global 4-step mechanism was based on the original CF2000 kinetic data and might be invalid when using the updated kinetics.

Reaction Kinetics

Figure 1 shows the investigated potential energy surface of the master equation used to compute the rate constants reported in the present work. In addition to the key reactions shown in Figure 1, the formulation included competing pathways for the fate of QOOH and OQ'OOH. These pathways are not shown, since their rate constants are not significant in the present work. The different colors indicate separated master equation formulations due to differences in the potential energy surface or the number of fragments. The additional

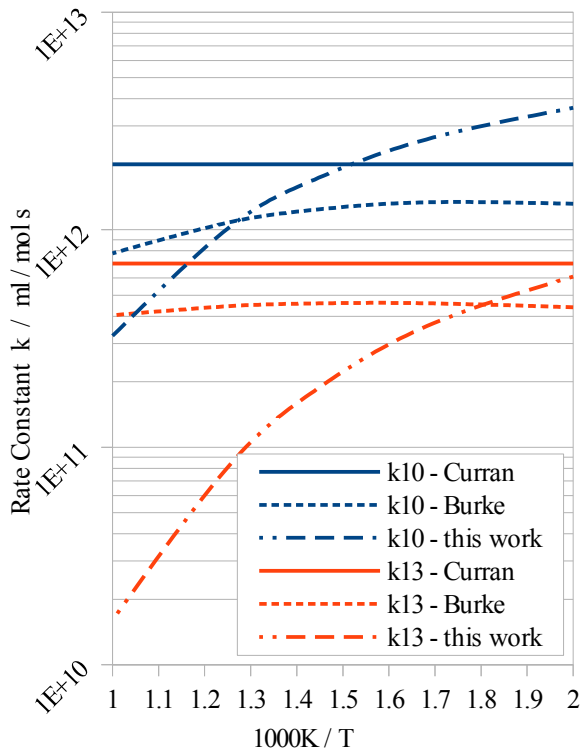

Figure 2: Bimolecular rate constants of the two oxygen addition steps. The solid lines are taken from the CF2000 model [21, 22] and the dashed lines are taken from the model of Burke *et al.* [23]. The dash-dotted lines were computed in the present work.

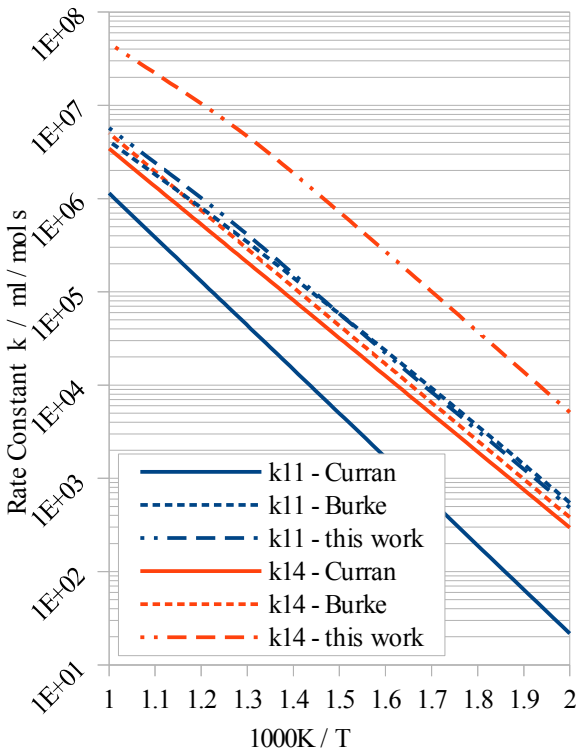

Figure 3: Unimolecular rate constants of the relevant isomerization reactions. The solid lines are taken from the CF2000 model [21, 22] and the dashed lines are taken from the model of Burke *et al.* [23]. The dash-dotted lines were computed in the present work.

energy due to the second O_2 addition is included by the E_{O2} term to allow for displaying all species on the same potential energy surface. The dashed horizontal line represents the reference energy of R + O_2 and all energy values are relative to this reference. The rate constants discussed in the present work are all at a pressure of 13 bar.

In Figure 2, the bimolecular rate constants k_{10} and k_{13} of the two O_2 addition reactions are shown in comparison to the rate constants used in the CF2000 model [21, 22] and used in the model of Burke *et al.* [23]. The first O_2 addition reaction (k_{10}) is essential for low-temperature chemistry, since it produces RO_2, which in turn is the key for separating high- and low-temperature chemistry. In the CF2000 model, this reaction is described by a temperature independent rate constant taken from O_2 addition reactions to alkyl radicals. Burke *et al.* [23] used the O_2 addition to propyl computed by Goldsmith *et al.* [34]. As can be seen from the dash-dotted curve for R + O_2 in Figure 2, the temperature dependence of the first O_2 addition rate constant of DME is much stronger than for similar reactions of alkyl radicals. Compared to the Burke *et al.* model, the addition is approx. a factor of two greater at low temperatures and approx. a factor of two smaller at high-temperatures. This leads to faster production of RO_2 below approx. 770 K, but slower production of RO_2 above. In case of the second O_2 addition reaction (k_{13}), the difference to previous rate constants amounts to more than one order of magnitude at high temperatures. This difference may be related to the smaller number of vibrational modes in DME as opposed to propane, which increases the dissociation rate and thus decreases the stabilization probability. Since this step initializes the chain branching part of the low-temperature network, the strong temperature dependence has a significant impact on the 'shape' of the NTC region. This impact on the ignition delay time will be discussed in the context of the rate constant for the competing fate of QOOH (k_{12} vs. k_{13}) later on.

In Figure 3, the unimolecular rate constants k_{11} and k_{14} of the two internal hydrogen abstraction reactions are shown in comparison to the rate constants used in the CF2000 model [21, 22] and used in the model of Burke *et al.* [23]. While using a lower level of theory, the RO_2 to QOOH isomerization rate of Burke *et al.* [23] is similar to the rate computed in the present work. Using a higher level of theory and treating internal modes as coupled hindered rotors leads to a different temperature dependence of the presented isomerization rate constant. Compared to similar reactions of hydrocarbons, the high isomerization rate is due to the ether oxygen and is a key to understanding the short ignition delay times of DME. The second

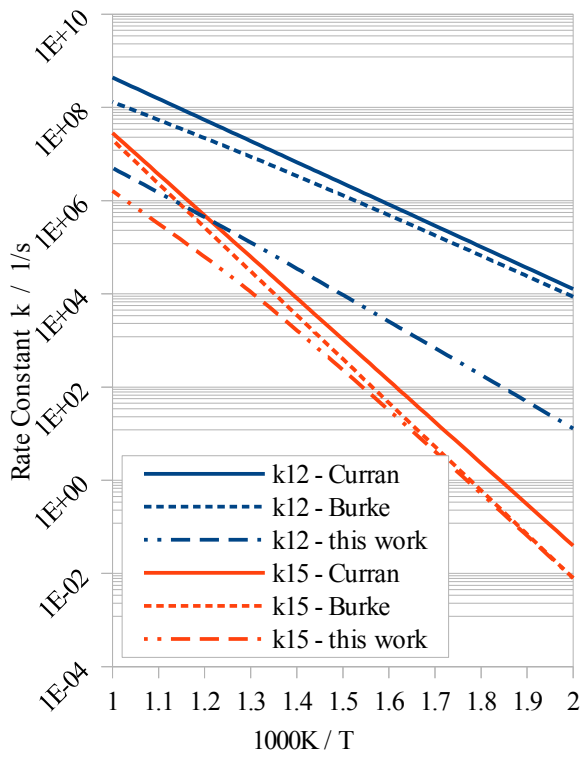

Figure 4: Unimolecular rate constants of OH loss reactions. The solid lines are taken from the CF2000 model [21, 22] and the dashed lines are taken from the model of Burke *et al.* [23]. The dash-dotted lines were computed in the present work.

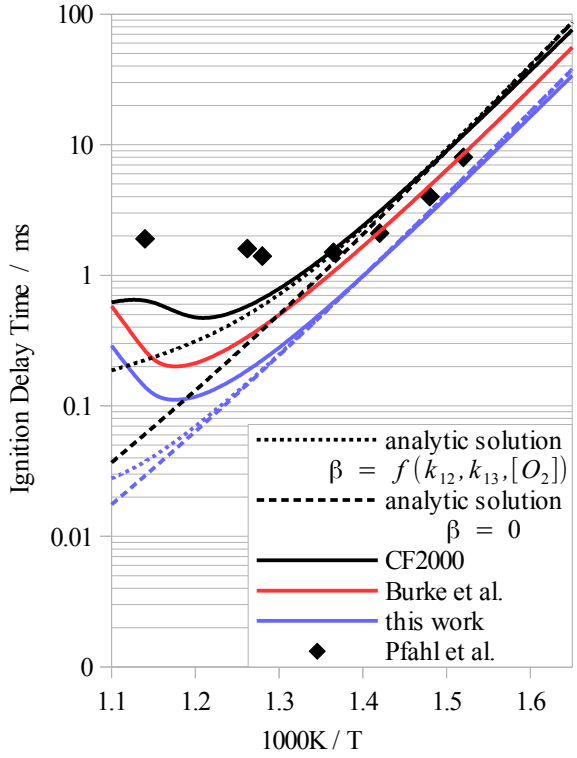

Figure 5: First-stage ignition delay time of dimethyl ether at 13 bar. Analytic ignition delay times and the solution of an updated 36-step mechanism of the CF2000 model [21, 22] are compared to the original model, the Burke *et al.*[23] model and experiments [2].

isomerization rate constant computed in the present work is about one order of magnitude higher than implemented in the Burke *et al.* and CF2000 model. Thus, the lifetime of O_2QOOH is shorter than assumed in previous models. Therefore, the respective isomer is formed faster and subsequent reactions are less delayed. As a consequence, the ignition delay time becomes shorter.

In Figure 4, the unimolecular rate constants k_{12} and k_{15} of the two OH loss reactions are shown in comparison to the rate constants used in the CF2000 model [21, 22] and used in the model of Burke *et al.* [23]. The updated rate constants show slower dissociation. While the second OH loss is only slightly slower than predicted in previous models, the first OH loss is lower by more than an order of magnitude in the present model. This reaction (k_{12}) is competing with the second O_2 addition reaction (k_{13}) (*cf.* Figure 2). The fate of QOOH determines the shape of the low-temperature regime of the ignition delay time. While at high temperatures the difference between the presented rate constants and previously used rate constants is almost the same for k_{12} and k_{13}, at low temperatures previous O_2 addition rates and the presented O_2 addition rates are approximately equal. Therefore, the O_2 addition is pronounced at low temperatures when using the present rate constants. Consequently, the low-temperature ignition delay time decreases and the S-shape of the NTC region becomes stronger.

Ignition Delay Times

We used the kinetic parameters of the 6 reactions updated in the present work for computing the analytic ignition delay time and for solving the 36-step mechanism. The latter was based on the CF2000 model [21, 22], while replacing the low-temperature pathway with the present data. We compared the results of the updated mechanism to simulation results of the original 36-step CF2000 model and the recent model of Burke *et al.* [23]. In Figure 5, the performance of each of these models is tested against experimental ignition delay time data of the first stage ignition at 13 bar.

While the CF2000 model over-predicts the ignition delay at temperatures below approx. 800 K, the Burke et al. model predicts the right order of magnitude. The remaining issues cannot be approached by partly updating previous models, but by performing a full modeling study. Instead, we aim for evaluating the impact of updating key reactions on the low-temperature ignition delay time of DME. When replacing previous rate constants with high-level quantum mechanical data, the remaining deviation from experimental data is assumed to be due to inaccuracies

of the remaining model.

Similar to the Burke *et al.* [23] model, the updated kinetics lead to predicting ignition delay times shorter than predicted by the original CF2000 model. In case of the Burke *et al.* model, the predicted ignition delay is shorter due to the faster RO_2 to QOOH isomerization. While the present isomerization rate is similar to that of Burke *et al.*, the addition rates differ significantly from the CF2000 model in the present work. Although the O_2 addition reactions were predicted to be smaller than previously, the high isomerization rates and the small rate constants for the first OH loss pronounce chain branching. Therefore, the predicted ignition delay is even shorter than predicted by the Burke *et al.* model.

Conclusions

The new kinetics provided for the low-temperature chemistry of dimethyl ether were compared to the kinetics used in the model of Fischer and Curran [21, 22] and used in the model of Burke *et al.* [23]. The updated rate constants presented here agree with previous data in some cases, but reveal deviations up to one order of magnitude for the O_2 addition reactions, the first OH loss and the second isomerization. Updating the key reactions of the low-temperature network lead to significant differences in the prediction of ignition delay times when updating the model of Fischer and Curran. Similar to the predictions of Burke *et al.*, the presented update of the Fischer/Curran model leads to shorter ignition delay time predictions.

The fact that updated kinetics, which are based on high-level quantum mechanics, leads to significant deviations from previous predictions and experimental ignition delay times reveals the need for a holistic approach when updating model data. Therefore, not only the forward rate constants of the backbone low-temperature reactions have to be updated, but also the thermochemistry and competing pathways.

Improving the low-temperature network of dimethyl ether by adding competing pathways for the fate of QOOH and OQ'OOH will be the next step with respect to updating existing combustion models. Furthermore, the effect of non-Boltzmann reactant distributions will be evaluated. Preliminary investigations point toward a significant impact on the second OH loss even at engine relevant conditions.

Acknowledgements

This work was performed as part of the Cluster of Excellence “Tailor-Made Fuels from Biomass” and the Aachen Institute for Advanced Study in Computational Engineering Science, which are both funded by the German Excellence Initiative. The work of Stephen J. Klippenstein was supported by the U.S. Department of Energy, Office of Science, Office of Basic Energy Sciences, Division of Chemical Sciences, Geosciences, and Biosciences under Contact No. DE-AC02-06CH11357. The support is gratefully acknowledged.

References

[1] A.M. Rouhi, Chem. Eng. News 73 (1995) 37-39
[2] U. Pfahl, K. Fieweger and C. Adomeit, Int. Symp. Combust. 26 (1996) 781-789
[3] P. Dagaut, C. Daly, J.M. Simmie and M. Cathonnet, Int. Symp. Combust. 26 (1998) 361-369
[4] G. Mittal, M. Chaos, C.-J. Sung and R.L. Dryer, Fuel Proc. Tech. 89 (2008) 1244-1254
[5] R.D. Cook, D.F. Davidson and R.K. Hanson, Proc. Combust. Inst. 32 (2009) 189-196
[6] Z. Chen, C. Tang, J. Fu, X. Jiang, Q. Li, L. Wei and Z. Huang, Fuel 102 (2012) 567-573
[7] L. Pan, E. Hu, J. Zhang, Z. Zhang, Z. Huang, Combust. Fuel 161 (2014) 735-747
[8] J. Sehested, K. Sehested, J. Platz, H. Egsgaard and O.J. Nielsen, Int. J. Chem. Kin. 29 (1997) 627-636
[9] I. Liu, N.W. Cant, J.H. Bromly, F.J. Barnes, P.F. Nelson and B.S. Haynes, Chemosphere 42 (2001) 583-589
[10] C.M. Rosado-Reyes, J.S. Francisco, J.J. Szente, M.M. Maricq and L.F. Ostergaard, J. Phys. Chem. A 109 (2005) 10940-10953
[11] H. Xu, C. Yao, T. Yuan, K. Zhang and H. Guo, Combust. Flame 158 (2011) 1673-1681
[12] J. Gao and Y. Nakumara, Fuel 106 (2013) 241-248
[13] T. Yamada, J.W. Bozzelli and T.H. Lay, Int. J. Chem. Kin. 32 (2000) 435-452
[14] A. Andersen and E.A. Carter, Israel J. Chem. 42 (2002) 245-260
[15] A. Andersen and E.A. Carter, J. Phys. Chem. A 107 (2003) 9463-9478
[16] A. Andersen and E.A. Carter, J. Phys. Chem. A 110 (2006) 1393-1407
[17] A. Andersen and E.A. Carter, Mol. Phys. 106 (2008) 367-396
[18] A.J. Eskola, S.A. Carr, R. Shannon, B.-S. Wang, M.A. Blitz, M.J. Pilling, P. Seakins and S.H. Robertson, J. Phys. Chem. A 118 (2014) 6773
[19] J. Beeckmann, L. Cai, A. Berens, N. Peters and H. Pitsch, Proc. Combust. Inst. 35 (2014) 275-281
[20] H.J. Curran, W.J. Pitz, C.K. Westbrook, P. Dagaut, J.-C. Boetner and M. Cathonnet, Int. J. Chem. Kin. 30 (1998) 229-241
[21] H.J. Curran, S.L. Fischer and F.L. Dryer, Int. J. Chem. Kin. 32 (2000) 741-759
[22] S.L. Fischer, F.L. Dryer and H.J. Curran, Int. J. Chem. Kin. 32 (2000) 713-740
[23] U. Burke, K.P. Somers, P. O'Toole, C.M. Zinner, N. Marquet, G. Bourque, E.L. Petersen, W.K. Metcalfe, Z. Serinyel and H.J. Curran, Combust. Flame 162 (2015) 315-330
[24] A.S. Tomlin, E. Agbro, V. Nevrlý, J. Dlabka and

M. Vasinek, Int. J. Chem. Kinet. 46 (2014), 662-682
[25] Y. Georgievskii, J.A. Miller, M.P. Burke and S.J. Klippenstein, J. Phys. Chem. A 117 (2013) 12146-12154
[26] Gaussian 09, Revision D.01, Gaussian Inc. Wallingford (2009)
[27] MOLPRO, version 2012.1, a package of ab initio programs, Cardiff, UK (2012)
[28] D.W. Schwenke, J. Chem. Phys. 122 (2005) 014107
[29] J.G. Hill, K.A. Peterson, G. Knizia and H.-J. Werner, J. Chem. Phys. 131 (2009) 194105
[30] Y. Georgievskii and S.J. Klippenstein, J. Phys. Chem. A 107 (2003) 9776-9781
[31] Y. Georgievskii and S.J. Klippenstein, J. Chem. Phys. 118 (2003) 5442
[32] J. Finley, P.-A. Malmqvist, B.O. Roos and L. Serrano-Andrés, Chem. Phys. Let. 288 (1998) 299-306
[33] H. Pitsch, FlameMaster, Version 3.31 (2008)
[34] C.F. Goldsmith, W.H. Green and S.J. Klippenstein, J. Phys. Chem. A 116 (2012) 3325-2246